Double-peak specific heat and spin freezing in the spin-2 triangular lattice antiferromagnet $FeAl_2Se_4$

Kunkun Li,[1,2] Shifeng Jin,[1,3] Jiangang Guo,[1] Yanping Xu,[1] Yixi Su,[5] Erxi Feng,[5] Yu Liu,[6] Shengqiang Zhou,[6] Tianping Ying,[7] Shiyan Li,[7,9,10] Ziqiang Wang,[11,*] Gang Chen,[7,8,10,†] and Xiaolong Chen[1,3,4,‡]

[1]*Beijing National Laboratory for Condensed Matter Physics, Institute of Physics, Chinese Academy of Sciences, Beijing 100190, China*
[2]*University of Chinese Academy of Sciences, Beijing 100049, China*
[3]*School of Physical Sciences, University of Chinese Academy of Sciences, Beijing 101408, China*
[4]*Collaborative Innovation Center of Quantum Matter, Beijing, China*
[5]*Juelich Centre for Neutron Science (JCNS) at Heinz Maier-Leibnitz Zentrum (MLZ), Forschungszentrum Juelich GmbH, Lichtenbergstr. 1, 85747 Garching, Germany*
[6]*Helmholtz-Zentrum Dresden-Rossendorf, Institute of Ion Beam Physics and Materials Research, Bautzner Landstraße 400, 01328 Dresden, Germany*
[7]*State Key Laboratory of Surface Physics, Department of Physics, Fudan University, Shanghai 200433, China*
[8]*Department of Physics and Center of Theoretical and Computational Physics, The University of Hong Kong, Pokfulam Road, Hong Kong, China*
[9]*Laboratory of Advanced Materials, Fudan University, Shanghai 200433, China*
[10]*Collaborative Innovation Center of Advanced Microstructures, Nanjing University, Nanjing 210093, China*
[11]*Department of Physics, Boston College, Chestnut Hill, Massachusetts 02467, USA*

(Received 4 June 2018; revised manuscript received 29 January 2019; published 19 February 2019)

We report the properties of a triangular lattice iron-chalcogenide antiferromagnet $FeAl_2Se_4$.The spin susceptibility reveals a significant antiferromagnetic interaction with a Curie-Weiss temperature $\Theta_{CW} \simeq -200$ K and a spin-2 local moment. Despite a large spin and a large $|\Theta_{CW}|$, the low-temperature behaviors are incompatible with conventional classical magnets. No long-range order is detected down to 0.4 K. Similar to the well-known spin-1 magnet $NiGa_2S_4$, the specific heat of $FeAl_2Se_4$ exhibits a double-peak structure and a T^2 power law at low temperatures, which are attributed to the underlying quadrupolar spin correlations and the Halperin-Saslow modes, respectively. The spin freezing occurs at $\sim$14 K, below which the relaxation dynamics is probed by the ac susceptibility. Our results are consistent with the early theory for the spin-1 system with Heisenberg and biquadratic spin interactions. We argue that the early proposal of the quadrupolar correlation and gauge glass dynamics may be well extended to $FeAl_2Se_4$. Our results provide useful insights about the magnetic properties of frustrated quantum magnets with high spins.

DOI: 10.1103/PhysRevB.99.054421

I. INTRODUCTION

Magnetic frustration arises in systems with competing spin interactions that cannot be optimized simutaneously [1]. In general, sufficiently strong frustration could lead to degenerate or nearly degenerate classical spin states and thus induce exotic and unconventional quantum states of matter such as quantum spin liquids when the quantum-mechanical nature of the spins is considered. The conventional wisdom and belief tells us that it is more likely to find these quantum states in magnetic systems with spin-1/2 degrees of freedom on frustrated lattices where quantum fluctuations are deemed to be strong. This explains the major efforts and interests in the spin-1/2 triangular lattice magnets such as Cs_2CuCl_4 [2,3], κ-$(BEDT\text{-}TTF)_2Cu_2(CN)_3$ [4–6], $EtMe_3Sb[Pd(mit)_2]_2$ [7], and $YbMgGaO_4$ [8–15], the spin-1/2 kagome lattice magnets such as herbertsmithite $ZnCu_3(OH)_6Cl_2$, volborthite [16] $Cu_3V_2O_7(OH)_2 \cdot 2H_2O$, and kapellasite [17] $Cu_3Zn(OH)_6Cl_2$, various spin-1/2 rare-earth pyrochlore magnets [18], and other geometrically frustrated lattices with spin-1/2 moments or effective spin-1/2 moments [19]. Despite the tremendous efforts in the spin-1/2 magnets, the magnets with higher spin moments can occassionally be interesting. The exceptional examples of this kind are the well-known Haldane phase [20,21] for the spin-1 chain and its high dimensional extension such as topological paramagnets [22,23]. The former has been discovered in various Ni-based one-dimensional magnets [24–26]. Another well-known example is the spin-1 triangular lattice antiferromagnet [27–29] $NiGa_2S_4$, where the biquadratic spin interaction [30–32], completely absent for spin-1/2 magnets, brings the spin quadrupolar order/correlation (or spin nematic) physics and phenomena into the system. Therefore, what matters is not just the size of the spin moment, but rather the interactions among the local moments and the underlying lattices. $FeGa_2S_4$, a spin-2 triangular lattice antiferromagnet that is isostructural with $NiGa_2S_4$, also shows the spin quadrupolar order/correlation (or spin nematic) physics and phenomena [28].

*wangzi@bc.edu
†gangchen.physics@gmail.com
‡chenx29@iphy.ac.cn

Inspired by the potentially rich physics in high-spin systems, in this paper, we study a spin-2 triangular lattice antiferromagnet $FeAl_2Se_4$ with both polycrystalline and single-crystalline samples. Analogous to the Ni^{2+} local moments in $NiGa_2S_4$ [27–29], the Fe^{2+} local moments in this material form a perfect triangular lattice and provide a perfect setting to explore the quantum physics of high spin moments on frustrated lattice. We find that the Fe local moments remain disordered down to 0.4 K despite a rather large antiferromagnetic Curie-Weiss temperature $\Theta_{CW} \simeq -200$ K. The magnetic susceptibility of single-crystal samples shows a bifurcation at about 14 K for field-cooling and zero-field-cooling measurements, suggesting a glassylike spin freezing. This is further assured from the ac susceptibility measurements at different probing frequencies. The specific heat of $FeAl_2Se_4$ shows a double-peak structure at two well-separated temperatures, indicating two distinct physical processes are occurring. Below the spin freezing temperature, a T^2 power-law specific heat is observed. Based on the early theoretical works [30–33] on $NiGa_2S_4$, we propose that the double-peak structure in heat capacity arises from the growth of correlation of two distinct types of spin moments, and the T^2 power law is the consequence of the Goldstone-type spin waves (i.e., the Halperin-Saslow modes). We further suggest that the spin freezing is due to the disorder that may induce the gauge glass physics into the would-be ordered state of this system.

The remaining parts of the paper are organized as follows. In Sec. II, we provide the data and the measurements of the crystal structure for $FeAl_2Se_4$. In Sec. III, we explain the thermodynamic measurements on this material. In Sec. IV, we focus on the specific heat and point out the double-peak structure in the specific heat and the low-temperature power-law behavior. In Sec. V, based on the dc susuceptibility, we further demonstrate the spin freezing from the ac susceptibility measurement. In Sec. VI, we discuss the broad impact and relevance of the physics in $FeAl_2Se_4$ to other systems and point out the future experiments.

II. CRYSTAL STRUCTURE

Our polycrystalline and single-crystal $FeAl_2Se_4$ samples were prepared from the high-temperature reactions of high-purity elements Fe, Al, and Se. In Fig. 1(a), we show the room-temperature x-ray diffraction pattern on the powder samples that are obtained by grinding the single-crystal samples. All the reflections could be indexed with the lattice parameters $a = b = 3.8335(1)$ Å, $c = 12.7369(5)$ Å. The systematic absences are consistent with space group $P\bar{3}m1$ (No. 164) isostructural to the previously reported compound $NiGa_2S_4$ [27]. The structural parameters are listed in Table I in Appendix B. In Fig. 1(b), we show the x-ray diffraction pattern of the single-crystal samples. It clearly indicates that the cleaved surface of the flaky crystal is the (001) plane and normal to the crystallographic c axis. The composition was examined by an inductively coupled plasma atomic emission spectrometer, giving the atomic ratios of Fe:Al:Se close to 1:2:4. The compound is built by stacking of layers consisting of edge-sharing $FeSe_6$ octahedra that are connected by a top and a bottom sheet of $AlSe_4$ tetrahedra. The layers are separated from each other by a van der Waals gap. The central

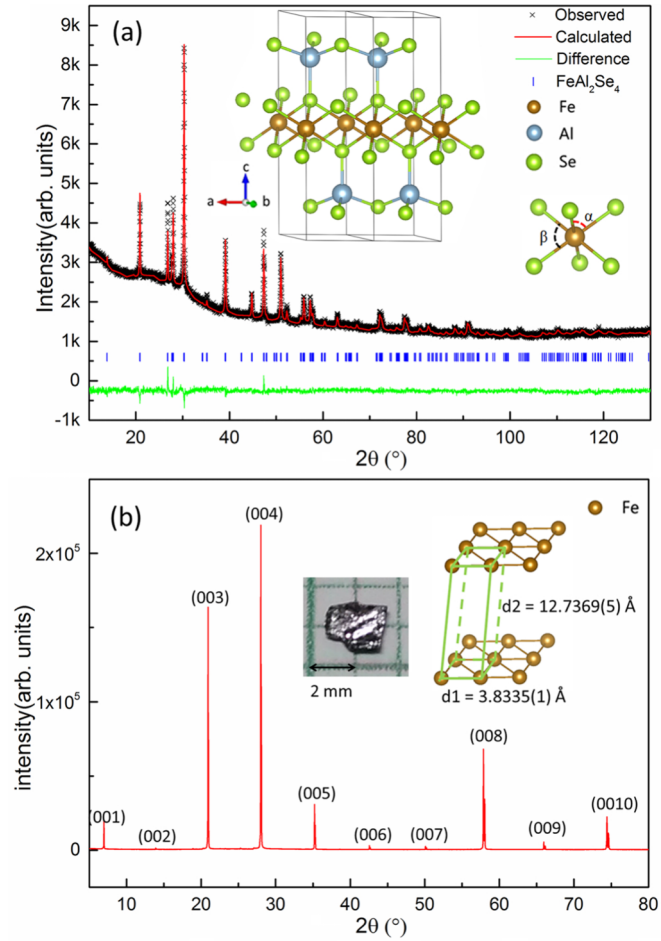

FIG. 1. (a) Powder x-ray diffraction and Rietveld refinement profile of $FeAl_2Se_4$ room temperature. The inset shows the schematic crystal structure of $FeAl_2Se_4$ and the distorted $FeSe_6$ octahedra. (b) The x-ray diffraction pattern of $FeAl_2Se_4$ crystal indicates that the (00l) reflections dominate the pattern. The inset shows the photography of $FeAl_2Se_4$ crystal with a length scale of 2 mm and an exhibition of the Fe sublattice.

$FeSe_6$ octahedra layer is isostructural to the CoO_2 layer of the well-known superconducting material [34] $Na_xCoO_2 \cdot yH_2O$.

In the crystal field environment of $FeAl_2Se_4$, the Fe^{2+} ion has an electronic configuration $t_{2g}^4 e_g^2$ that gives rise to a high spin state and a spin $S = 2$ local moment. The six Fe-Se bonds are of equal length and are 2.609(3) Å. Se-Fe-Se angles are 94.55(8)°, marked as α, and 85.45(8)°, marked as β, as displayed in the inset of Fig. 1(b). The different Se-Fe-Se angles represent a slight rhombohedral distortion of the $FeSe_6$ octahedra, resulting in a small crystal field splitting among the t_{2g} orbitals. The degenerate or nearly degenerate t_{2g} orbitals and the partially filled t_{2g} shell may lead to an active orbital degree of freedom. This will be further discussed from the magnetic entropy measurement.

Finally, in $FeAl_2Se_4$, the nearest intralayer Fe-Fe distance is $d_1 = 3.8335(1)$ Å and the nearest interlayer Fe-Fe distance is $d_2 = 12.7369(5)$ Å, indicating an ideal two-dimensional character in terms of the lattice structure.

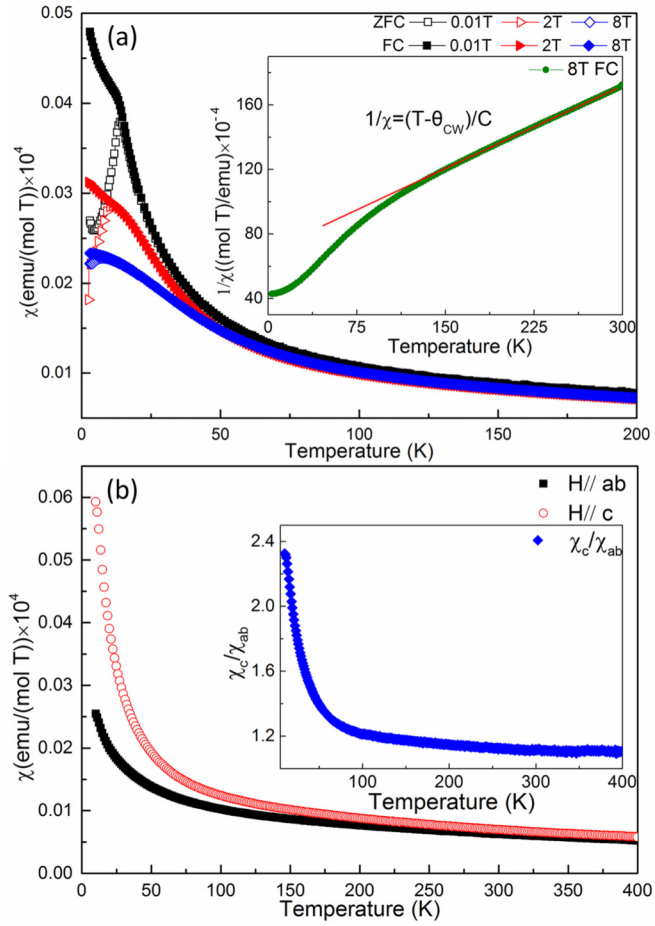

FIG. 2. (a) Zero-field-cooled (ZFC) and field-cooled (FC) $\chi(T)$ data taken at different applied fields from 2 to 300 K. Inset: the inverse susceptibility $\chi^{-1}(T)$ data with the applied field of 8 T. The solid red lines are linear fits with a Curie-Weiss law $\chi = C/(T - \Theta_{\rm CW})$. (b) Temperature dependence of the magnetic susceptibility χ_{ab} and χ_c obtained for $FeAl_2Se_4$ under 0.1 T from 10 to 400 K. Inset: the ratio of χ_c/χ_{ab} vs T.

III. THERMODYNAMIC MEASUREMENTS

To identify the magnetic properties of $FeAl_2Se_4$, we first implement the thermodynamic measurements. The temperature-dependent dc magnetic susceptibility and its inverse χ^{-1} under the external magnetic fields of 0.01, 2, and 8 T are shown in Fig. 2. A bifurcation (denoted as T_f) at 14 K can be seen under a field of 0.01 T, and can be suppressed down to 8 K when the applied field is raised up to 8 T. This is a signature of spin freezing. The temperature-dependent susceptibility from 150 to 300 K obeys a simple Curie-Weiss law $\chi = C/(T - \Theta_{\rm CW})$, where C is the Curie constant and $\Theta_{\rm CW}$ is the Weiss temperature as illustrated in the inset of Fig. 2(a). The effective magnetic moments, 4.80–5.20μ_B, were obtained from the Curie constants. The Weiss temperature $\Theta_{\rm CW} = -200$ K, which is more negative than that for the isostructural material [28] $FeGa_2S_4$ ($\Theta_{\rm CW} = -160$ K), indicates stronger antiferromagnetic interactions. When the temperature is lower than 150 K, $FeAl_2Se_4$ shows a deviation from the Curie-Weiss behavior. The frustration index, defined by $f = |\Theta_{\rm CW}/T_f|$ with T_f the spin freezing temperature, is estimated as 14. This is a relatively large value, and we thus conclude that $FeAl_2Se_4$ is a magnetically frustrated system. Figure 2(b) shows the magnetic susceptibility measurements of $FeAl_2Se_4$ single crystals with $H \parallel ab$ (χ_{ab}) and $H \parallel c$ (χ_c). Unlike $NiGa_2S_4$ and $FeGa_2S_4$ [28], here we find an easy-axis anisotropy with χ_c/χ_{ab} about 2.4 at 10 K instead of easy-plane anisotropy. This is due to the partially filled t_{2g} shell in the Fe^{2+} ion where the spin-orbit coupling is active and induces the anisotropy in the spin space.

The magnetic heat capacity after subtracting the phonon contributions is used to reveal the spin contribution. The heat capacity of an isostructural nonmagnetic material $ZnIn_2S_4$ is measured to account for the lattice contribution of $FeAl_2Se_4$. We obtained the thermal variation of the Debye temperature $\Theta_D(T)$ using the Debye equation. $\Theta_D(T)$ of $FeAl_2Se_4$ was then estimated by applying a scale factor according to $\Theta_D(T) \propto M_0^{-1/2} V_0^{-1/3}$, where M_0 and V_0 are molar mass and volume, respectively. Thus, the lattice contribution C_L was estimated by the scaled $\Theta_D(T)$ data. The magnetic part, C_m, was then estimated through subtracting the lattice contributions C_L [27]. No clear anomaly associated with any magnetic transition can be detected from the specific heat data down to 0.4 K, indicating a ground state without any true long-range spin ordering. Similar to $NiGa_2S_4$ and $FeGa_2S_4$ [28], $FeAl_2Se_4$ exhibits a double-peak variation of C_m/T: one at $\sim$10 K, and the other at $\sim$65 K, as shown in Fig. 3(a). We will revisit the double-peak structure of the heat capacity later.

The magnetic entropy, $S_m(T) = \int_0^T C_m/T\, dT$, increases gradually over the entire measured temperature range but with a plateau near $T \sim 25$ K, indicating high degeneracy of low-energy states due to magnetic frustration. The total entropy reaches $R\ \ln(5)$ at $T \sim 135$ K, corresponding to the value for the $S = 2$ system. Then it further increases toward $R\ \ln(15) = R\ \ln(5) + R\ \ln(3)$. The latter term is from the orbital degree of freedom due to two holes present in the t_{2g} orbitals [28]. The low-temperature part of C_m/T, as shown in Fig. 3(b), displays a near linear T dependence around 4 K and then deviates from the line with further increasing temperature, similar to the behavior that was observed in $NiGa_2S_4$ and $FeGa_2S_4$. In addition, the linear-T coefficient γ for C_m/T of 5.9 mJ/mol K^2 at $T \to 0$ K can be obtained for $FeAl_2Se_4$, slightly larger than that in $FeGa_2S_4$ (3.1 mJ/mol K^2). The observed T^2 specific heat can be attributed to the Halperin-Saslow modes [35] in two dimensions that give a specific heat of the form

$$C_m = N_{\rm A} \frac{3\pi k_B V}{c} \left[\zeta(3) \sum_j \left(\frac{k_B T}{\pi \hbar v_j} \right)^2 - \frac{1}{L_0^2} \right], \qquad (1)$$

where $V = \sqrt{3}a^2 c/2$ is the unit-cell volume with a the Fe-Fe spacing, L_0 is the coherence length for the spin excitations, and v_j is the velocity in the jth direction. From $C_m/T^2 = 0.010$ J/mol K^3, the estimated average v_j is 1400 m/s. For ordinary antiferromagnets that order at $T \sim \Theta_{\rm CW}$, the average v_j is estimated as

$$v_j^2 \approx [3\sqrt{3}\zeta(3)/4\pi](a k_{\rm B} \Theta_{\rm CW}/\bar{h})/\ln(2S+1), \qquad (2)$$

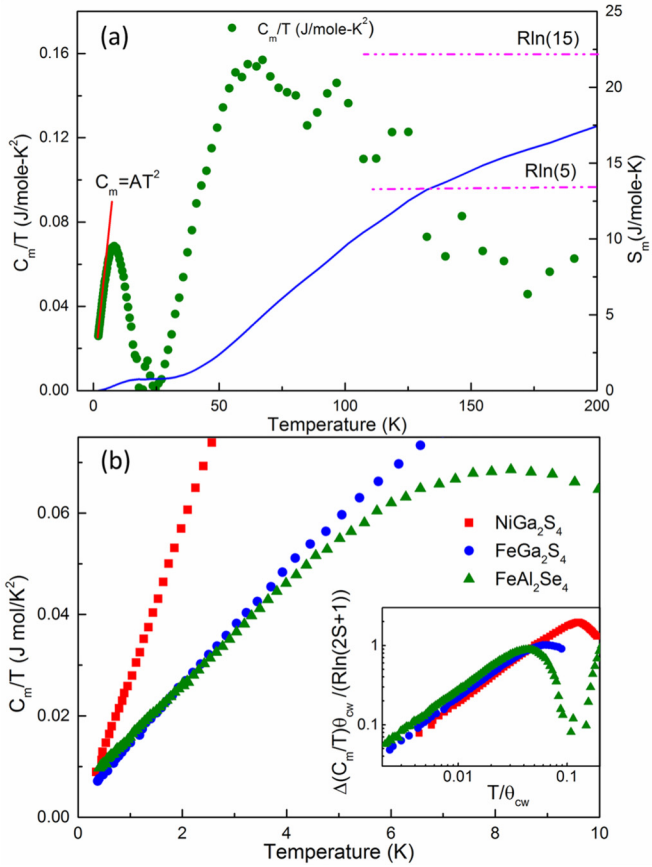

FIG. 3. (a) Temperature dependence of magnetic entropy (right axis) and C_m/T (left axis) for $FeAl_2Se_4$. (b) The low-temperature part of magnetic heat capacity C_m/T for $NiGa_2S_4$, $FeGa_2S_4$, and $FeAl_2Se_4$. The inset shows the $\Delta(C_m/T)\Theta_{CW}/[R\ \ln(2S+1)]$ vs T/Θ_{CW} for $NiGa_2S_4$ ($S=1$, $\Theta_{CW}=-80$ K), $FeGa_2S_4$ ($S=2$, $\Theta_{CW}=-160$ K), and $FeAl_2Se_4$ ($S=2$, $\Theta_{CW}=-200$ K) at 0 T in full logarithmic scale.

which gives $v_j \approx 5600$ m/s. The smaller value in our case indicates softening due to the magnetic frustration, and is consistent with $NiGa_2S_4$ and $FeGa_2S_4$ [27–29]. Using the susceptibility data $\chi(T\to 0)=0.0025$ emu/mol, the estimated spin stiffness $\rho_s=\chi(v/\kappa)^2=49.5$ K, where $\kappa=g\mu_B/\hbar$, which is larger than those obtained in $FeGa_2S_4$ ($\rho_s=35.8$ K) and $NiGa_2S_4$ ($\rho_s=6.5$ K). To further compare $FeAl_2Se_4$ with the other two counterparts, the inset of Fig. 3(b) shows $\Delta(C_m/T)\Theta_{CW}/[R\ \ln(2S+1)]$ vs T/Θ_{CW} for $NiGa_2S_4$ ($S=1$, $\Theta_{CW}=-80$ K), $FeGa_2S_4$ ($S=2$, $\Theta_{CW}=-160$ K), and $FeAl_2Se_4$ ($S=2$, $\Theta_{CW}=-200$ K) at zero field (0 T) in full logarithmic scale, where $\Delta(C_m/T)\Theta_{CW}=C_m/T-\gamma$. As shown in Fig. 3(b), the low-temperature data for $FeAl_2Se_4$ nearly collapse on top of $NiGa_2S_4$ and $FeGa_2S_4$, indicating similar Halperin-Saslow modes present in all three compounds.

IV. DOUBLE-PEAK HEAT CAPACITY

Here we discuss the origin of the double-peak structure in the heat capacity of $FeAl_2Se_4$. As noted, such a double-peak structure was first observed in the spin-1 magnet $NiGa_2S_4$ [27]. The theoretical studies have invoked a spin

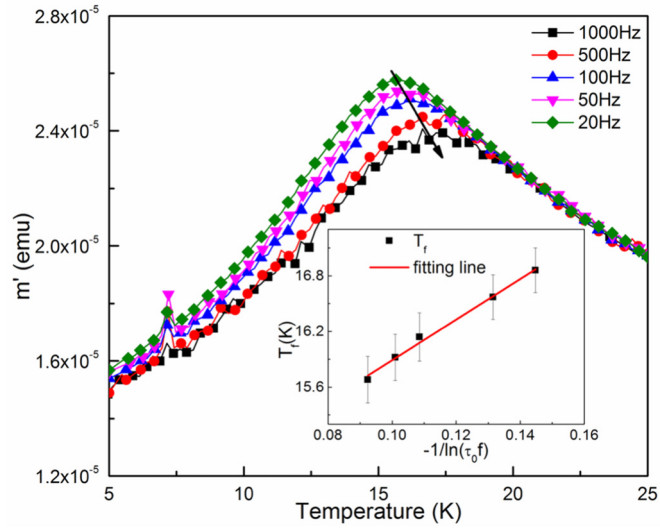

FIG. 4. Temperature dependence of the real part of the ac magnetic susceptibility as a function of frequency. It should be noted that the small peak emerging at approximately 7 K is frequency independent; the origin is unknown.

model with both Heisenberg and biquadratic exchange interactions [30–32], where the biquadratic exchange interaction $-(\boldsymbol{S}_i\cdot\boldsymbol{S}_j)^2$ arises from the spin-lattice coupling. Since $FeAl_2Se_4$ is isostructural to $NiGa_2S_4$, we expect a similar model and interactions to apply. The presence of the biquadratic exchange allows the system to access the spin quadrupole moments effectively and hence enhance the quadrupolar correlation. In addition to the usual magnetic (dipole) moment S^μ, both spin-1 and spin-2 moments support the quadrupole moments,

$$Q_{\mu\nu}=\tfrac{1}{2}(S^\mu S^\nu+S^\nu S^\mu)-\tfrac{1}{3}S(S+1)\delta_{\mu\nu} \qquad (3)$$

with $\mu=x,y,z$. Since the quadrupole and dipole moments are quite distinct and have different symmetry properties, they ought to behave differently. Moreover, it is the biquadratic interaction that directly couples the quadrupole moments of different sites. It was then argued and shown numerically [30] that the system develops significant quadrupolar correlations at a distinct higher temperature than the one associated with the rapid growth of the magnetic correlations when the system is close to the quantum phase transition from spiral (dipolar) spin order to quadrupolar order. These two temperature scales associated with the rapid growth of magnetic and quadrupolar correlations result in a double-peak structure of the heat capacity. Based on the fact that $FeAl_2Se_4$ has an identical lattice structure and an even larger spin Hilbert space, we expect the same mechanism to account for the double-peak heat capacity in $FeAl_2Se_4$.

V. SPIN FREEZING AND ac SUSCEPTIBILITY

To further characterize the low-temperature magnetic properties of $FeAl_2Se_4$ at temperatures near the spin freezing, we measure the temperature-dependent ac susceptibility from 5 to 25 K for a number of frequencies. As shown in Fig. 4, a peak in the real part at $\sim$15 K is present, which is the signature of the susceptibility bifurcation. A small but clear peak shift

toward high temperatures can be observed when the probing frequency is increased. This suggests a spin-relaxation behavior. The shift of the peak temperature as a function of frequency described by the expression $(\Delta T_f)/(T_f \Delta \log \omega)$ is usually used to distinguish spin-glass and spin-glass-like materials [36,37]. The value obtained for $FeAl_2Se_4$ is 0.042, which is slightly larger than expected for a canonical spin glass but is in the range of spin-glass-like materials.

Usually the spin freezing with the glassy behavior is due to the disorder and/or frustration that are present in $FeAl_2Se_4$. Like the S vacancies in $NiGa_2S_4$, we suspect the Se vacancies to be the dominant type of impurities and sources of disorder. Without disorders, the system may simply develop the spin density or spiral magnetic orders. With (nonmagnetic bond) disorders, the phase transition associated with the discrete lattice symmetry breaking would be smeared out in $FeAl_2Se_4$. No sharp transition was observed in the heat capacity measurement on $FeAl_2Se_4$. By assuming a complex XY order parameter for each magnetic domain in the spin freezing regime, the authors in Ref. [30] invoked a phenomenological gauge glass model [38,39] where the complex orders from different magnetic domains couple with the disorder in a fashion similar to the coupling with a random gauge link variable. They propose that the system would realize a gauge glass ground state, and the Goldstone-type spin waves in a long-range ordered state turn into the Halperin-Saslow modes [33,35] in the gauge glass model. These gapless modes in two dimensions contribute to the T^2 specific heat [35] in the spin freezing regime. Due to the phenomenological nature of the model, we think the gauge glass model and the conclusion should also describe and apply to the low-temperature physics in the spin freezing regime of $FeAl_2Se_4$.

VI. DISCUSSION

Although the large spin moments tend to behave more classically than spin-1/2 moments, the large spin moments have a larger spin Hilbert space and would allow more possibilities for the quantum ground states. If the interaction can access these Hilbert spaces effectively, interesting quantum states may be stabilized. From our experimental results in $FeAl_2Se_4$, we find that the system exhibits a two-peak structure in the heat capacity. We argue that these two peaks correspond to the separate growth of quadrupolar correlation and magnetic (dipolar) correlation. From the early experience with the spin-1 triangular lattice magnet $NiGa_2S_4$ [27–33], we expect this physics is certainly not exclusive to $FeAl_2Se_4$, and it is not even exclusive to spin-2 magnets or to triangular lattice magnets. This type of physics, i.e., the rich moment structure and their correlations, may broadly exist in frustrated magnets with high spin moments if the interaction can access these high-order multipole moments effectively. In the cases of $FeAl_2Se_4$ and $NiGa_2S_4$, it is the spin-lattice-coupling induced biquadratic interaction that enhances the quadrupolar order and correlation. Besides these two known examples, for other high spin systems such as the $4d/5d$ magnets [40,41] and $4f$ rare-earth magnets [42–45], the spin-orbit coupling and entanglement could induce strong multipolar interaction and provide another mechanism to access and enhance the quadrupolar (and more generally multipolar) spin orders and correlations. Thus, we think our results and arguments could stimulate interests in frustrated magnets with high spins and rich moment structures.

To be specific to $FeAl_2Se_4$, there are a couple of directions for future experiments. Since the biquadratic interaction is suggested to arise from the spin-lattice coupling, it is useful to substitute some Se with S to modify the spin-lattice coupling and hence the biquadratic interaction. This should affect the quadrupolar correlation and the specific heat. Neutron-scattering measurement can be quite helpful to probe both the low-energy modes like the Halperin-Saslow modes and the spin correlation in different temperature regimes [46]. Nuclear magnetic resonance and muon spin resonance experiments can also be useful to reveal the dynamical properties of the system at different temperatures. On the theoretical side, it would be interesting to establish a general understanding and a phase diagram of a spin-2 model with both Heisenberg and biquadratic interactions on the triangular lattice.

ACKNOWLEDGMENTS

This work is financially supported by Key Research Program of Frontier Sciences, CAS, Grant No. QYZDJ-SSW-SLH013; the National Natural Science Foundation of China under Grants No. 51532010, No. 51772323, No. 91422303, No. 51472266, No. 2016YFA0301001, and No. 2016YFA0300500 (G.C.); and the DOE, Basic Energy Sciences Grant No. DE-FG02-99ER45747 (Z.Q.W.).

APPENDIX A: MATERIALS AND METHODS

Polycrystalline samples of $FeAl_2Se_4$ were prepared by the reaction of Fe (99.99%, Alfa-Aesar), Al (99.95%, Alfa-Aesar), and Se (99.999%, Shiny) powders. These reagents were intimately ground together using an agate pestle and mortar and placed in an alumina crucible. The crucible was placed inside a quartz tube which was evacuated, sealed, and partially backfilled with ultrahigh-purity argon. The samples were fast heated at 500 °C for 8 h, then kept at 900 °C for

TABLE I. Room-temperature structure details of $FeAl_2Se_4$.

Space group	$P\bar{3}m1$ (164)
a (Å)	3.8336(1)
c (Å)	12.7369(5)
V (Å^3)	162.11(1)
Atomic parameters	
Fe(1b)	(0,0,1/2)
Al(2d)	[1/3,2/3, 0.2001(8)]
Se1(2d)	[1/3,2/3, 0.8658(4)]
Se2(2d)	[1/3,2/3,0.3915(3)]
Selected bond lengths and angles	
d Fe-Se (Å)	2.609(3)
α Se-Fe-Se (deg)	94.55(8)
β Se-Fe-Se (deg)	85.45(8)
Agreement factors	
R_p	2.29%
R_{wp}	2.94%

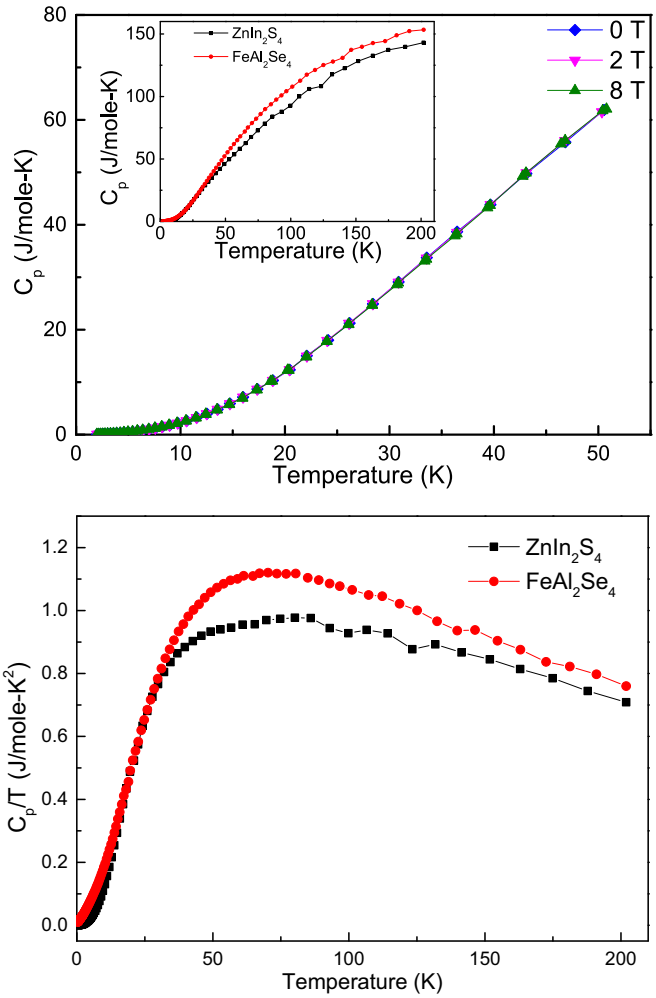

FIG. 5. The specific heat data measured at different fields. Inset of (a): Temperature dependence of specific heat for $FeAl_2Se_4$ and $ZnIn_2S_4$ between 200 and 0.4 K.

several days, and finally cooled naturally to room temperature by switching off the furnace. Crystals were prepared by the reaction of Fe (99.99%, Alfa-Aesar) pieces, Al (99.95%, Alfa-Aesar) wire, and Se (99.999%, Shiny) shot in an appropriate molar ratio. These reagents were simply put together in an alumina crucible. Similar to the procedure for preparing the polycrystalline sample, the growth of crystals was performed at 1070 °C for a duration of 24 h and then cooled slowly

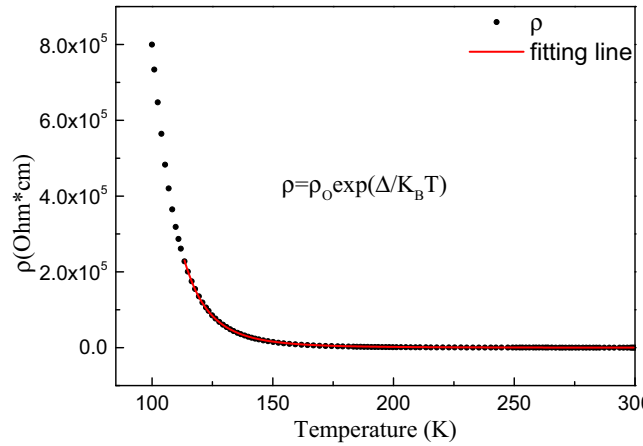

FIG. 6. Temperature dependence of the resistivity $\rho(T)$ of $FeAl_2Se_4$. Red line indicates the fitting results of $\rho(T)$ using the thermal activation model.

to 470 °C then naturally cooled down to room temperature by switching off the furnace. All measurements performed on the powder sample were grounded from the single-crystal sample. dc magnetization and heat capacities were measured on a physical properties measurement system (PPMS) using the relaxation technique. Resistivity was measured on a PPMS using the standard four-probe configuration. ac magnetization was measured on a magnetic properties measurement system (Quantum Design) using powders.

APPENDIX B: THE STRUCTURE DETAILS OF $FeAl_2Se_4$

In Table I, we list the detailed structure information about $FeAl_2Se_4$.

APPENDIX C: SPECIFIC HEAT FOR $FeAl_2Se_4$, $ZnIn_2S_4$ AND RESISTIVITY OF $FeAl_2Se_4$

In Fig. 5, we plot the temperature dependence of the specific heat of $FeAl_2Se_4$ at various fields. In addition, the result for the nonmagnetic material $ZnIn_2S_4$ is also provided.

In Fig. 6, we provide the variation of resistivity with temperature for $FeAl_2Se_4$. An insulating ρ vs T dependence is clearly seen. The $\rho(T)$ obeys the thermally activated behavior $\rho = \rho_0 \exp(E_a/k_BT)$, where E_a is the activation energy with fitted value of 0.106 eV, consistent with the black color of the compound.

[1] L. Balents, Spin liquids in frustrated magnets, Nature (London) **464**, 199 (2010).

[2] R. Coldea, D. A. Tennant, and Z. Tylczynski, Extended scattering continua characteristic of spin fractionalization in the two-dimensional frustrated quantum magnet Cs_2CuCl_4 observed by neutron scattering, Phys. Rev. B **68**, 134424 (2003).

[3] R. Coldea, D. A. Tennant, A. M. Tsvelik, and Z. Tylczynski, Experimental Realization of a 2D Fractional Quantum Spin Liquid, Phys. Rev. Lett. **86**, 1335 (2001).

[4] Y. Shimizu, K. Miyagawa, K. Kanoda, M. Maesato, and G. Saito, Spin Liquid State in an Organic Mott Insulator with a Triangular Lattice, Phys. Rev. Lett. **91**, 107001 (2003).

[5] Y. Kurosaki, Y. Shimizu, K. Miyagawa, K. Kanoda, and G. Saito, Mott Transition from a Spin Liquid to a Fermi Liquid in the Spin-Frustrated Organic Conductor κ-$(ET)_2Cu_2(CN)_3$, Phys. Rev. Lett. **95**, 177001 (2005).

[6] S. Yamashita, Y. Nakazawa, M. Oguni, Y. Oshima, H. Nojiri, Y. Shimizu, K. Miyagawa, and K. Kanoda, Thermodynamic properties of a spin-1/2 spin-liquid state in a kappa-type organic salt, Nat. Phys. **4**, 459 (2008).

[7] T. Itou, A. Oyamada, S. Maegawa, M. Tamura, and R. Kato, Spin-liquid state in an organic spin-1/2 system on a triangular lattice, $EtMe_3Sb[Pd(dmit)_2]_2$, J. Phys.: Condens. Matter **19**, 145247 (2007).

[8] Y. Li, H. Liao, Z. Zhang, S. Li, F. Jin, L. Ling, L. Zhang, Y. Zou, L. Pi, Z. Yang, J. Wang, Z. Wu, and Q. Zhang, Gapless quantum spin liquid ground state in the two-dimensional spin-1/2 triangular antiferromagnet $YbMgGaO_4$, Sci. Rep. **5**, 16419 (2015).

[9] Y. Li, G. Chen, W. Tong, L. Pi, J. Liu, Z. Yang, X. Wang, and Q. Zhang, Rare-Earth Triangular Lattice Spin Liquid: A Single-Crystal Study of $YbMgGaO_4$, Phys. Rev. Lett. **115**, 167203 (2015).

[10] Y. Shen, Y.-D. Li, H. Wo, Y. Li, S. Shen, B. Pan, Q. Wang, H. C. Walker, P. Steffens, M. Boehm, Y. Hao, D. L. Quintero-Castro, L. W. Harriger, L. Hao, S. Meng, Q. Zhang, G. Chen, and J. Zhao, Spinon Fermi surface in a triangular lattice quantum spin liquid $YbMgGaO_4$, Nature (London) **540**, 559 (2016).

[11] J. A. M. Paddison, Z. Dun, G. Ehlers, Y. Liu, M. B. Stone, H. Zhou, and M. Mourigal, Continuous excitations of the triangular-lattice quantum spin liquid $YbMgGaO_4$, Nat. Phys. **13**, 117 (2017).

[12] Y.-D. Li, Y.-M. Lu, and G. Chen, Spinon Fermi surface $U(1)$ spin liquid in the spin-orbit-coupled triangular-lattice Mott insulator $YbMgGaO_4$, Phys. Rev. B **96**, 054445 (2017).

[13] J. Iaconis, C. Liu, G. B. Halász, and L. Balents, Spin liquid versus spin orbit coupling on the triangular lattice, SciPost Phys. **4**, 003 (2018).

[14] Z. Zhu, P. A. Maksimov, S. R. White, and A. L. Chernyshev, Disorder-Induced Mimicry of a Spin Liquid in $YbMgGaO_4$, Phys. Rev. Lett. **119**, 157201 (2017).

[15] Y.-D. Li, Y. Shen, Y. Li, J. Zhao, and G. Chen, Effect of spin-orbit coupling on the effective-spin correlation in $YbMgGaO_4$, Phys. Rev. B **97**, 125105 (2018).

[16] Z. Hiroi, M. Hanawa, N. Kobayashi, M. Nohara, H. Takagi, Y. Kato, and M. Takigawa, Spin-1/2 *Kagomé*-like lattice in Volborthite $Cu_3V_2O_7(OH)_2{\cdot}2H_2O$, J. Phys. Soc. Jpn. **70**, 3377 (2001).

[17] B. Fåk, E. Kermarrec, L. Messio, B. Bernu, C. Lhuillier, F. Bert, P. Mendels, B. Koteswararao, F. Bouquet, J. Ollivier, A. D. Hillier, A. Amato, R. H. Colman, and A. S. Wills, Kapellasite: A Kagome Quantum Spin Liquid with Competing Interactions, Phys. Rev. Lett. **109**, 037208 (2012).

[18] J. S. Gardner, M. J. P. Gingras, and J. E. Greedan, Magnetic pyrochlore oxides, Rev. Mod. Phys. **82**, 53 (2010).

[19] Y. Okamoto, M. Nohara, H. Aruga-Katori, and H. Takagi, Spin-Liquid State in the $S = 1/2$ Hyperkagome Antiferromagnet $Na_4Ir_3O_8$, Phys. Rev. Lett. **99**, 137207 (2007).

[20] F. D. M. Haldane, Nonlinear Field Theory of Large-Spin Heisenberg Antiferromagnets: Semiclassically Quantized Solitons of the One-Dimensional Easy-Axis Néel State, Phys. Rev. Lett. **50**, 1153 (1983).

[21] I. Affleck, T. Kennedy, E. H. Lieb, and H. Tasaki, Rigorous Results on Valence-Bond Ground States in Antiferromagnets, Phys. Rev. Lett. **59**, 799 (1987).

[22] X. Chen, Z.-C. Gu, Z.-X. Liu, and X.-G. Wen, Symmetry-protected topological orders in interacting bosonic systems, Science **338**, 1604 (2012).

[23] C. Wang, A. Nahum, and T. Senthil, Topological paramagnetism in frustrated spin-1 Mott insulators, Phys. Rev. B **91**, 195131 (2015).

[24] W. J. L. Buyers, R. M. Morra, R. L. Armstrong, M. J. Hogan, P. Gerlach, and K. Hirakawa, Experimental Evidence for the Haldane Gap in a Spin-1 Nearly Isotropic, Antiferromagnetic Chain, Phys. Rev. Lett. **56**, 371 (1986).

[25] Y. Ajiro, T. Goto, H. Kikuchi, T. Sakakibara, and T. Inami, High-Field Magnetization of a Quasi-One-Dimensional $S = 1$ Antiferromagnet $Ni(C_2H_8N_2)_2NO_2(ClO_4)$: Observation of the Haldane Gap, Phys. Rev. Lett. **63**, 1424 (1989).

[26] A. P. Ramirez, S-W. Cheong, and M. L. Kaplan, Specific Heat of Defects in Haldane Systems Y_2 $BaNiO_5$ and NENP: Absence of Free spin-1/2 Excitations, Phys. Rev. Lett. **72**, 3108 (1994).

[27] S. Nakatsuji, Y. Nambu, H. Tonomura, O. Sakai, S. Jonas, C. Broholm, H. Tsunetsugu, Y. Qiu, and Y. Maeno, Spin disorder on a triangular lattice, Science **309**, 1697 (2005).

[28] S. Nakatsuji, H. Tonomura, K. Onuma, Y. Nambu, O. Sakai, Y. Maeno, R. T. Macaluso, and J. Y. Chan, Spin Disorder and Order in Quasi-2D Triangular Heisenberg Antiferromagnets: Comparative Study of $FeGa_2S_4$, $Fe_2Ga_2S_5$, and $NiGa_2S_4$, Phys. Rev. Lett. **99**, 157203 (2007).

[29] C. Stock, S. Jonas, C. Broholm, S. Nakatsuji, Y. Nambu, K. Onuma, Y. Maeno, and J.-H. Chung, Neutron-Scattering Measurement of Incommensurate Short-Range Order in Single Crystals of the $S = 1$ Triangular Antiferromagnet $NiGa_2\mathbf{S}_4$, Phys. Rev. Lett. **105**, 037402 (2010).

[30] E. M. Stoudenmire, S. Trebst, and L. Balents, Quadrupolar correlations and spin freezing in $S = 1$ triangular lattice antiferromagnets, Phys. Rev. B **79**, 214436 (2009).

[31] S. Bhattacharjee, V. B. Shenoy, and T. Senthil, Possible ferrospin nematic order in $NiGa_2S_4$, Phys. Rev. B **74**, 092406 (2006).

[32] H. Tsunetsugu and M. Arikawa, Spin nematic phase in $s = 1$ triangular antiferromagnets, J. Phys. Soc. Jpn. **75**, 083701 (2006).

[33] D. Podolsky and Y. B. Kim, Halperin-Saslow modes as the origin of the low-temperature anomaly in $NiGa_2S_4$, Phys. Rev. B **79**, 140402 (2009).

[34] R. E. Schaak, T. Klimczuk, M. L. Foo, and R. J. Cava, Superconductivity phase diagram of $Na_xCoO_2{\cdot}1.3H_2O$, Nature (London) **424**, 527 (2003).

[35] B. I. Halperin and W. M. Saslow, Hydrodynamic theory of spin waves in spin glasses and other systems with noncollinear spin orientations, Phys. Rev. B **16**, 2154 (1977).

[36] J. A. Mydosh, *Spin Glasses: An Experimental Introduction* (CRC Press, Boca Raton, FL, 1993).

[37] J. W. Krizan and R. J. Cava, $NaCaCo_2F_7$: A single-crystal high-temperature pyrochlore antiferromagnet, Phys. Rev. B **89**, 214401 (2014).

[38] D. S. Fisher and D. A. Huse, Equilibrium behavior of the spin-glass ordered phase, Phys. Rev. B **38**, 386 (1988).

[39] D. S. Fisher, M. P. A. Fisher, and D. A. Huse, Thermal fluctuations, quenched disorder, phase transitions, and transport in type-II superconductors, Phys. Rev. B **43**, 130 (1991).

[40] G. Chen, R. Pereira, and L. Balents, Exotic phases induced by strong spin-orbit coupling in ordered double perovskites, Phys. Rev. B **82**, 174440 (2010).

[41] G. Chen and L. Balents, Spin-orbit coupling in d^2 ordered double perovskites, Phys. Rev. B **84**, 094420 (2011).

[42] S. Onoda and Y. Tanaka, Quantum Melting of Spin Ice: Emergent Cooperative Quadrupole and Chirality, Phys. Rev. Lett. **105**, 047201 (2010).

[43] Y.-P. Huang, G. Chen, and M. Hermele, Quantum Spin Ices and Topological Phases from Dipolar-Octupolar Doublets on the Pyrochlore Lattice, Phys. Rev. Lett. **112**, 167203 (2014).

[44] Y.-D. Li, X. Wang, and G. Chen, Hidden multipolar orders of dipole-octupole doublets on a triangular lattice, Phys. Rev. B **94**, 201114 (2016).

[45] C. Liu, Y.-D. Li, and G. Chen, Selective measurements of intertwined multipolar orders: Non-Kramers doublets on a triangular lattice, Phys. Rev. B **98**, 045119 (2018).

[46] A. Smerald, H. T. Ueda, and N. Shannon, Theory of inelastic neutron scattering in a field-induced spin-nematic state, Phys. Rev. B **91**, 174402 (2015).